Study Methodology

This study includes 5 distinct investigations, in addition to the web platform design, which each follow their own methodology and are described below:
1. The identification and mapping of shallow insular features in the South China Sea
2. Bathymetry mapping
3. Sea level dynamics
4. Habitat classification and land cover mapping
5. Geographic description
6. The design of the web platforms to display the results

1. Identification and mapping of shallow insular features in the South China Sea

We used freely-available Landsat data at a resolution of 30mx30m to identify areas with exposed or shallow geographic features that require further detailed study using commercially available high resolution satellite data. The Landsat data is notated using Worldwide Reference System (WRS). Each scene is designated by Path and Row numbers. Our study area lies within Path numbers 117 to 123 and Row numbers 48 to 57. We scanned for visible features starting from the most recently acquired Landsat 8 data, followed by Landsat 7 and 5. The scenes used are shown in the table below.

Path/Row	Scene ID	Satellite
117.48	lc81170482014029	Landsat 8
117.49	lc81170492014029	Landsat 8
117.50	lc81170502014077	Landsat 8
117.51	lc81170512014317	Landsat 8
117.52	lc81170522014077	Landsat 8
117.53	lc81170532014077	Landsat 8
118.48	lt51180482004169	Landsat 5
118.49	lc81180492014260	Landsat 8
118.50	lc81180502014260	Landsat 8
118.51	lc81180512014260	Landsat 8
118.52	lc81180522014260	Landsat 8
118.53	lc81180532014260	Landsat 8
118.54	lc81180542014068	Landsat 8
118.55	lc81180552014068	Landsat 8
119.48	lt51190482009253	Landsat 5
119.49	le71190492000109	Landsat 7

119.49	lt51190491995087	Landsat 5
119.50	lt51190501995087	Landsat 5
119.52	lc81190522014027	Landsat 8
119.52	lc81190522014059	Landsat 8
119.52	lc81190522014107	Landsat 8
119.53	lc81190532013120lgn01	Landsat 8
119.54	lc81190542013120lgn01	Landsat 8
119.54	lc81190542014075	Landsat 8
119.55	lc81190552014075	Landsat 8
119.56	lc81190562014059	Landsat 8
120.48	le71200482014074	Landsat 7
120.49	lc81200492014002	Landsat 8
120.49	lc81200492014050	Landsat 8
120.50	lc81200502013303	Landsat 8
120.51	lc81200512013303	Landsat 8
120.52	lc81200522013143lgn01	Landsat 8
120.52	LC81200522014114	Landsat 8
120.52	lc81200522014226	Landsat 8
120.53	LC81200532014034	Landsat 8
120.53	LC81200532014066	Landsat 8
120.53	LC81200532014114	Landsat 8
120.54	LC81200542014226	Landsat 8
120.55	LC81200552014034	Landsat 8
120.56	lc81200562014130	Landsat 8
120.57	lc81200572014130	Landsat 8
121.48	lc81210482014073	Landsat 8
121.49	lc81210492014025	Landsat 8
121.49	lc81210492014137	Landsat 8

121.50	lc81210502014073	Landsat 8
121.51	lc81210512014073	Landsat 8
121.52	lt51210521996120	Landsat 5
121.53	lc81210532014073	Landsat 8
121.54	LC81210542014089	Landsat 8
121.54	LC81210542014217	Landsat 8
121.55	lc81210552014217	Landsat 8
121.56	lc81210562014073	Landsat 8
122.48	le71220482013021edc00	Landsat 7
122.49	lc81220492013141lgn01	Landsat 8
122.49	lc81220492014224	Landsat 8
122.49	lc81220492014272	Landsat 8
122.49	le71220492010045edc00	Landsat 7
122.50	le71220502014072	Landsat 7
122.51	le71220512014072	Landsat 7
122.51	lt51220512005071	Landsat 5
122.52	le71220522014072	Landsat 7
122.52	lt51220522004101	Landsat 5
122.53	lt51220532004101	Landsat 5
122.54	lc81220542014064	Landsat 8
122.55	lc81220552014064	Landsat 8
122.56	lt51220562004101	Landsat 5
123.48	lc81230482013180lgn00	Landsat 8
123.49	lc81230492014103	Landsat 8
123.49	lc81230492014215	Landsat 8
123.50	lc81230502014183	Landsat 8
123.51	lc81230512013228	Landsat 8
123.51	lc81230512014183	Landsat 8

123.52	lc81230522013228	Landsat 8
123.52	lc81230522014263	Landsat 8
123.53	lc81230532013340	Landsat 8
123.53	lc81230532014135	Landsat 8
123.54	lt51230541999318	Landsat 5

Features that had been identified in satellite imagery were compared with georeferenced nautical charts: 13 maps, indexed 17010 to 18800, published by the Navigation Guarantee Department of the Chinese Navy Headquarters (China) and 2 maps, indexed 61134 and 61136, published by Glavnoe upravlenie navigatsii i okeanografii (Russia). Full details of the charts is provided below.

Index No.	Name of Nautical Chart	Scale	Date published/ edited in red on hard-copy
17010	Xisha, Zhongsha Qundao	1:500,000	2006/2012
17030	Zhongsha Qundao to Nansha Qundao	1:500,000	2008/2010
17040	Mui Dinh to Cua Me Cong Song, Riji Jiao	1:500,000	2010/2012
17100	Xisha Qundao	1:250,000	2005/2012
18050	Northern and Central Portions of Nansha Qundao	1:800,000	2006/2012
18100	Shuangzi Qunjiao to Zhenghe Qunjiao	1:250,000	2013
18200	Liyue Tan	1:250,000	2013
18300	Yongshu Jiao to Yinqing Qunjiao	1:250,000	2013
18400	Zhenghe Qunjiao to Yongshu Jiao	1:250,000	2005/2010
18500	Nanfang Qiantan to Haikou Jiao	1:250,000	2005/2012
18600	Yinqing Qunjiao to Nanwei Tan	1:250,000	2012
18700	Wumie Jiao to Huanglu Jiao	1:250,000	2013
18800	Haikou Jiao to Yuya Ansha	1:250,000	2013
61134	South China Sea. Vanguard Shoal to North Luconia Shoals	1:500,000	2010
61136	South China Sea. Kalimantan. Tanjong Nosong to Batang Tatau	1:500,000	2008

Findings were also compared with lists of insular features in the South China Sea in the sources listed in the references below. The depth of those that were only faintly visible on Landsat imagery was verified on the above nautical charts and in the SRTM15 database. Those that were for the most part less than 10m were short-listed to be studied with high resolution satellite imagery. The final list of features examined is provided in the List of Shallow Geographic Features and the exhaustive list of satellite images consulted is available in the Table of Sources (Satellite Data).

References

1. <<南海诸岛地名资料汇编>>. 广东省地名委员会编, 出版: 广州 : 广东省地图出版社, 1987. Guangdong Province Committee on Geographical Names, 1987. A Collection of Nanhai Islands Geographic Names and Documents, Guangdong Province Map Press, Guangdong (China). pp 629.

2.《南沙群岛空间融会信息剖析与示警：群礁发育、军事区位、警示体系》作者：高俊国，刘宝银 著 出版社：海洋出版社 2009
Gao, Junguo and Liu, Baoyin, 2009. Spratly Islands space fusion and warning information analysis: Group reef development, military location, warning system. China Ocean Press. pp 172.

3. Hancox, D. and Prescott, J. R. V., 1995. A geographical description of the Spratly Islands and an account of hydrographic surveys amongst those islands. Maritime Briefing, 1(6) International Boundaries Research Unit.

4. Sailing Directions (Enroute) South China Sea and the Gulf of Thailand, Publication 161, U.S. Governement Printing Office (2013)

5. UK Admiralty Sailing Directions, China Sea Pilot (2010)

6. M.J. Valencia, J.M. Van Dyke, N.A. Ludwig, Sharing the Resources of the South China Sea, University of Hawaii Press, 1997

7. 2014 SRTM15 topography grid made available by the Scripps Institution of Oceanography, University of California San Diego: http://topex.ucsd.edu/WWW_html/srtm30_plus.html

8. S. Kakuta et al. (2010) Satellite-based Mapping of Coral Reefs in East Asia, Micronesia and Melanesia Regions, International Archives of the Photogrammetry, Remote Sensing and Spatial Information Science, Volume XXXVIII, Part 8, Kyoto Japan 2010 available at http://www.isprs.org/proceedings/XXXVIII/part8/pdf/W06D04_20100311190523.pdf and the corresponding coral reef layers in ArcGIS.

9. Office of the Geographer, US State Department, South China Sea Map and Gazetteer, 803425A1, January 2010 [accessible here]

2. Derivation of sea water depth from satellite images

This study uses high resolution multispectral satellite images to derive water depth and sea bottom albedo. Ideally, hyperspectral data (with tens or even hundreds of contiguous spectral bands) are best suited for modelling of light propagation in waters and for retrieving optical parameters, water depth and bottom albedo, as the complete water reflectance spectra are available for fitting with specific models of water reflectance. Since hyperspectral satellite data is not operationally available, we use the commercial high resolution multispectral satellite data (IKONOS, GeoEye-1, WorldView-2) for these purposes.

High spatial resolution satellite sensors are usually designed for land applications. These sensors typically have a small number of broad spectral bands. Despite the limited number of spectral bands, water depth and sea bottom albedo can still be derived with the incorporation of some suitable assumptions [1, 2].

Satellites

Most of the images used in this study were acquired by the WorldView-2 and GeoEye-1 satellites with 2m nominal resolution in the multispectral bands (Refer to this link for the full list of satellite data). The panchromatic band (0.5 m nominal resolution) from the same satellites were used to "pan-sharpen" the multispectral images to produce colour images at 0.5 m resolution. These pan-sharpened images have altered spectral values. They were used in visual interpretation but not in quantitative computation of water depth. A few IKONOS images (4 m resolution) were also used where the higher resolution satellite images were not available.

The imaging instrument on the GeoEye-1 satellite (launched in September 2008) has four multispectral bands (blue, green, red and NIR) at 1.65 m spatial resolution and a panchromatic band at 0.41 m resolution. The presence of the blue band enables derivation of bathymetry to a water depth of up to 20 m, especially in clear sea waters. The IKONOS satellite (launched September 1999) also has similar spectral bands, except that the resolution is 4 m for the multispectral bands and 1 m for the panchromatic band.

The WorldView-2 satellite (launched October 2009) has 8 multispectral bands at 1.84 meter resolution. Four of the bands are the "conventional" bands (blue, green, red and NIR1) similar to those present in GeoEye-1 and most other multispectral satellites. The additional 4 spectral bands ("coastal", yellow, "red edge" and NIR2) are the new bands. For consistency, only the conventional bands are used in this study.

Pre-processing

The light radiance detected by a space-borne sensor is the sum of several components due to the interactions of the downward solar and sky irradiance with the atmosphere, water surface, bulk water and sea bottom. The effects of all these interactions need to be modelled and corrected in order to derive the water leaving reflectance, which contains information about the water optical properties, water depth and the sea bottom characteristics.

The digital numbers of each spectral band of the satellite images are first converted to the effective in-band radiance using the calibration constants supplied by the satellite operators. The radiance is then converted to the top-of-atmosphere (TOA) reflectance by normalizing with the TOA solar irradiance [1]. The TOA reflectance is influenced by atmospheric effects, which include absorption by gaseous molecules as well as scattering by molecules and aerosol. In this study, the TOA reflectance is corrected for Rayleigh scattering and molecular absorption using routines in the 6S package [3], assuming a standard tropical atmosphere with considerations of the spectral response of each spectral band of the sensor.

The effects of surface glint and aerosol scattering is corrected by subtracting the reflectance of the NIR band from the other spectral bands. This procedure assumes that the water is dark in the NIR band. This assumption is generally valid for clear water, where there is no significant scattering due to suspended particulate matter such that light attenuation through water is predominantly due to absorption by water. For GeoEye-1, the NIR band absorption coefficient is 3.85 m^{-1} with an effective penetration depth of 26 cm. Hence, except for very shallow water and if the water is not very turbid, the water at the NIR band can be assumed to be dark so that the signal observed in this band (after Rayleigh

correction) is primarily due to aerosol scattering and surface glint only. The water leaving reflectance is obtained after the surface glint and aerosol correction. The water leaving reflectance The water leaving reflectance (measured above the water surface) is then converted to the sub-surface reflectance for subsequent derivation of water depth and bottom albedo.

Derivation of water depth and bottom albedo

The sub-surface shallow water reflectance r_i at the i-th spectral band is a sum of two components [1, 2, 4],

$$r_i = r_{wi}[1-\exp(-MK_iH)] + \frac{\rho_{bi}}{\pi}\exp(-MK_iH) .$$

The first component is due to scattering from the bulk water characterized by the deep water reflectance r_{wi}, which is related to the water absorption and backscattering coefficients, a_i and b_{bi}. The second component is related to the sea bottom reflectance ρ_{bi}. The other parameters common to both components are the water depth *H*, the effective attenuation coefficient $K_i \approx a_i + b_{bi}$, and the geometric path length factor *M*.

With a limited number of spectral bands, the above equation is mathematically unsolvable. Some simplifying assumptions are needed in order to solve this equation for water depth and bottom albedo. We first estimate the water absorption and backscattering coefficients a_i and b_{bi} at the deep water using an algorithm based on the Quasi-Analytical Algorithm (QAA) [5, 6, 7]. We assume that the water at the shallow region has the same optical properties as the deep water so the same a_i and b_{bi} can be applicable for shallow water [1].

At the shallow water region, we model the sea bottom reflectance by a reference sand reflectance,

$$\rho_{bi} = A\hat{\rho}_i$$

where $\hat{\rho}_i$ is the reference sand reflectance normalized to one at the green band, and *A* is the bottom surface albedo at the green band. Since M is a known geometric parameter, the two remaining unknowns are the water depth *H* and bottom albedo *A,* which can be obtained by numerically solving the shallow water reflectance equation at two spectral bands.

Post-processing

After the water depth map is derived, it is visually inspected and compared with the satellite image to mask out regions of low confidence which may be due to factors such as thin clouds, cloud shadows, haze, excessive glints that cannot be reliably corrected and rough sea states, among others. A size filter is applied to remove noise. Exposed land and other features are visually identified from the high NIR reflectance and verified using the pan-sharpened image.

Limitations

Glint correction – In certain cases, very shallow regions may appear slightly deeper due to overcorrection of glint and regions with very high surface glint may appear shallower due to under-correction.

Water clarity at the shallow water region – The water clarity at the shallow water region is assumed to be the same as that of the deep water. This is usually not an issue if the water is well circulated and no human activities are involved. However, if the water is turbid, it may appear shallower than it actually is.

Sea bottom effect – The sea bottom is modelled by a reference sand reflectance. This is not an issue if the spectral shape of the material covering the sea bottom surface is similar to that of the reference sand spectrum, which is usually the case. However if this assumption is violated, for example, where there are submerged vegetation, the water depth may appear deeper.

Unmasked clouds and waves – Clouds and waves are generally masked by visual inspection. The residual unmasked clouds and waves may result in variations in the derived water depth.

Cloud shadows - Regions under cloud shadows are masked manually. Any unmasked region under cloud shadows may appear deeper due to the relatively lower reflectance.

Image artefacts – Residual processing artefacts (such as banding) within any of the multispectral bands may result in slight variations of depth.

References

1. S. C. Liew, J. He, 2008. Uplift of a coral island in the Andaman Sea due to the 2004 Sumatra earthquake measured using remote sensing reflectance of water. IEEE Geosci. Remote Sens. Lett. 5(4), 701–704.

2. S. C. Liew, P. Chen, B. Saengtuksin, C. W. Chang, 2011. Estimating water optical properties, water depth and bottom albedo using high resolution satellite imagery for coastal habitat mapping, Proc. IEEE 2011 International Geoscience and Remote Sensing Symposium (IGARSS'11), 2338-2340.

3. E. Vermote, D. Tanre, J. L. Deuze, M. Herman, and J. J. Morcette, 1997. Second simulation of the satellite signal in the solar spectrum, 6S: An overview. *IEEE Trans. Geosci. Remote Sens.* 35(3), 675–686.

4. Z. P. Lee, K. L. Carder, C. D. Mobley, R. G. Steward, and J. S. Patch, 1999. Hyperspectral remote sensing for shallow waters. 2. Deriving bottom depths and water properties by optimization. *Appl. Opt.* 38(18), 3831–3843.

5. Z. P. Lee, K. L. Carder, R. Arnone, 2002. Deriving inherent optical properties from water color: a multiband quasi-analytical algorithm for optically deep waters. Appl. Opt. 41, 5755–5772.

6. International Ocean Colour Coordinating Group (IOCCG), 2006. Remote sensing of Inherent optical properties: Fundamentals, tests of algorithms, and applications. Lee, Z.-P. (ed.), Reports of the International Ocean-Colour Coordinating Group, No. 5, Dartmouth, Canada. (Available online: http://www.ioccg.org/reports/report5.pdf)

7. D. S. van Maren, S. C. Liew, and G. M. J. Hasan, 2014. The role of terrestrial sediment on turbidity near Singapore's coral reefs. *Continental Shelf Research* 76, 75-88.

3. Sea Level dynamics

Sea levels have been calculated for each shallow insular feature identified in the South China and summarised in a set of three graphs. The significance of sea level variations (under the combined effect of astronomic tides and wind) is explained below, as well as the methodology followed.

Ocean *astronomic tides* are the rise and fall of sea levels caused by the combined effects of gravitational forces exerted by the Moon, Sun, and rotation of the Earth. Forced by changing solar and lunar gravitational potential, tides propagate around the Earth's oceans in form of waves that manifest themself at tidal gauge records as harmonic oscillations. The stronger are the forces, the higher the *tidal range* defined as difference between sea levels at tidal wave crest and trough.

The sea level varies due to tides at different time scales – from hourly to decadal. When ocean water rises to its highest level due to tidal forces, it reaches *high tide* (i.e., high water). While it falling to its lowest level, it is called *low tide* (i.e. low water). At most Earth's locations, theoretically closer to the Equator, there are two high tides and two low tides each lunar day (roughly 24 hours and 50 minutes) due to interplay of gravitational and centrifugal forces. Such a pattern is called a *semidiurnal tide*. Near the Polar Regions, a *diurnal tide* has a usual pattern of one high and one low tide each lunar day. Due to existence of continents and uneven coastal line, the patterns often distorted from the idealized theory to form a *mixed tide*, having both features simultaneously.

During *spring tides* the range is the highest due to mutual reinforcement of the gravitational forces of the Sun and Moon at new moon or full moon phases. *Neap tides* have the lowest range due to mutual partial cancelation of the gravitational forces of the Sun and Moon when their vectors toward the Earth form a right angle. It is observed during the first and last quarters of the moon's phases. Both spring and neap tides happen approximately twice a month. The *largest annual tidal range* can be expected around the time of the equinox, if coincidental with a spring tide. Tidal parameters are normally defined over a significantly long period of time, ideally the full Metonic cycle of 18.6 years. *Mean Sea Level* (MSL) is defined as long-term mean of sea water record at a particular location.

Tidal records at a particular point could be linearly decomposed to a few principle *tidal constituents*, each represented by a cosine shaped wave characterized by an amplitude, a period (or a frequency over its wave length), and a phase shift relative to Greenwich Mean Time (GMT). The combined oscillation is further distorted and modulated by continental alignment, uneven water depth and interaction with atmospheric forcing (wind and air pressure), resulting in different sea levels at different geographical locations. Atmospheric forces may cause higher or lower sea level than predicted according to tidal forces alone.

<u>Derivation of sea level in the South China Sea</u>

In the South China Sea, sea level at spring tide may reach about 2 meters at some locations. It means, for instance, that a rock that stands 1.8 meter high above the water at the lowest level would be fully submerged during the highest level. In the context of shallow and flat coral formations, this 2-meter variation between highest and lowest tides is sufficient to fully cover or uncover such a coral establishment. This variability impacts both the intertidal life that may live on it and the legal statute of this area as possible 'naturally formed area of land above water at high tide'.

Across the world, variations in sea level are measured on site with tidal gauges permanently installed along the coasts. However, one of the obstacles facing the understanding of tides in the SCS and particularly their variations on insular features such as the seamounts of the Spratly is the lack of available real time measurements in the region. Therefore, in the

project, tide is predicted using FES2012, one of the most accurate global ocean tide models. The model assimilated long time series of altimetry data (Topex/Poseidon, Jason-1, Jason-2, ERS-1, ERS-2 and Envisat satellites) into a high-resolution (1/16°×1/16°) hydrodynamic model. Its spectra consist of 11 main constituents (namely M2, S2, K1, O1, N2, K2, P1, Q1, S1, 2N2 and Ssa), 8 minor components (E2, J1, L2, La2, Mu2, Nu2, R2 and T2), 4 long period tides (Mf, Mm, MSf and Mtm) and 9 shallow non-linear ones (M3, M4, M6, M8, N4, MS4, MN4, S4 and MKS2). Predicted tide for a geographical coordinate is obtained at hourly interval throughout 20 years, starting from 00:00 GMT+0 hour of the 1st January 2000 to 23:00 the 31st of December. Mean Sea Level in FES2012 model is set to zero.

For the historical events in the South China Sea, sea level predicted using tide model is corrected using observed sea level anomaly from satellite altimetry data (AVISO) to account for the meteorological effects. The AVISO data are gridded at the resolution (1/4°×1/4°) on the daily basis since 00:00 GMT+0 the 1st January 2000 to the 11st September 2015. For the future event, sea level is adjusted in accordance with meteorological effect using daily climatology of AVISO altimetry data. Here the climatology is derived by taking daily average over its entire period.

Tidal graphs and related notations

The sea level graphs below provide a sample of the graphs created for each feature.

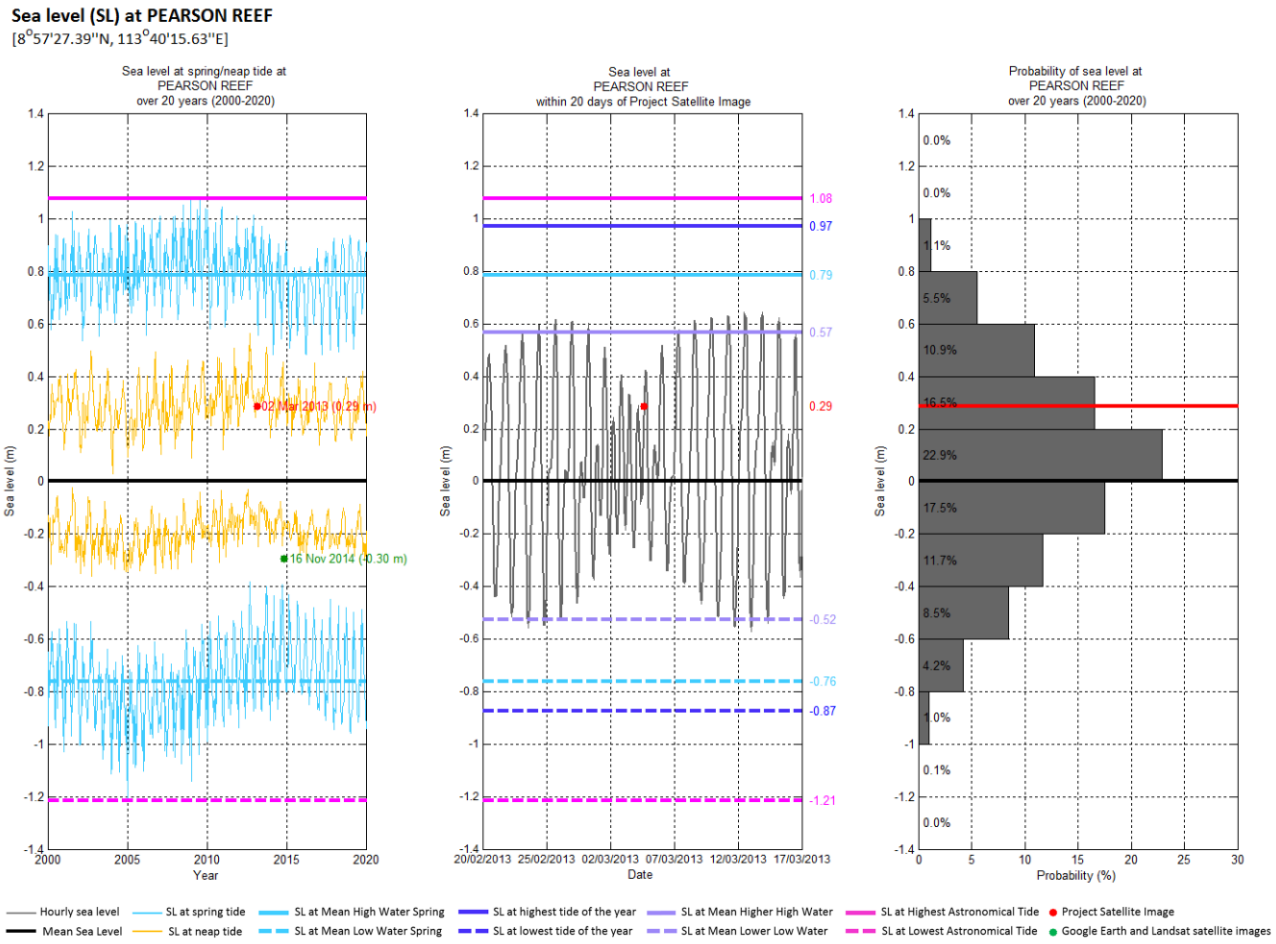

Sea level at spring tide is defined as an average of two successive extremes (both highest or both lowest) during spring tide. *Sea level at neap tide* is defined as an average of two

successive extremes (both highest or both lowest) during neap tide. Both definitions include influences of tidal and meteorological forces on sea level.

Mean High Water Spring (MHWS) is defined as an average of (abovementioned) *sea levels at spring tides* over a long period (which is 20 years long in this study). Similarly, *Mean Low Water Spring* (MLWS) is defined as an average of *sea levels at neap tide*.

Higher High Water (HHW) is defined as the highest sea level during a lunar day, which due to a combined influence of tidal and meteorological forces. *Sea level at Mean Higher High Water* (MHHW) is defined as an average of HHWs over a long period. In reverse, *Lower Low Water* (LLW) is defined as the lowest sea level during a lunar day, and *sea level at Mean Lower Low Water* (MLLW) is thus defined as an average of LLWs over a long period.

Highest Astronomical Tide (HAT) is defined as the highest sea level to occur due to astronomic tide. In practice, *sea level at HAT* is defined as the highest extreme to occur over a long period, which is inclusive of meteorological influence. *Lowest Astronomical Tide* (LAT) is similarly defined as the lowest sea level to occur due to astronomic tide; whereas *sea level at LAT* is defined as the lowest sea level extremes to occur over a long period.

Limitations

There is no observation of sea level at the insular features in the South China except the two stations administrated by China hourly record are unavailable for public use. Hence, sea level was predicted using FES2012 tide model which in our preliminary analysis has an error of about 5-10cm with the sea level decomposed from harmonic analysis of tidal record at select stations located on the coasts of South East Asian countries. The discrepancy is mainly due to the inadequate resolution of FES2012 in resolving very fine insular features in the South China Sea and the missing of seasonal components (such as SSA, SA) in its tidal spectra coverage.

The discrepancy between our predicted sea level and actual observation is also caused the unavoidable inaccuracy of sea level anomaly observed from satellite data, which is daily mean and coarse resolution.

4. Habitat classification

A semi-automated object oriented image classification method was developed for mapping the costal and marine habitats in the South China Sea using the very high resolution (2-meter) satellite multispectral imagery (WorldView2, WorldView3, GeoEye-1 and QuickBird-2 and Ikonos-2; Refer to this link for the full list of satellite data).

Pre-processing of satellite images

The satellite images were first converted from digital numbers (DN) to the top of atmosphere (TOA) spectral radiance and reflectance using the band calibration coefficients provided in the image metadata files. The TOA reflectance was then corrected for Rayleigh scattering and gaseous absorption in the atmosphere. Sun glint effects, the specular reflection of light from water surfaces, were also removed from the images.

Thematic classification of coastal and marine habitats

In this project, the object-based image analysis (OBIA) (Blaschke, 2010; Benz et al., 2004) was used for the mapping using the eCognition software.

First, the multiresolution segmentation algorism (Baatz and Schäpe, 2000; Trimble eCognition, 2015) was used for feature extraction that is a bottom-up region-merging technique, the smaller image objects with similar spectral and spatial characteristics were

merged into larger objects in an iterative optimization procedure based on the defined scale, shape and compactness parameters. The spectral difference segmentation algorism (Trimble eCognition, 2015) was also performed to refine the segmentation results. The relatively homogeneous and semantically significant objects were generated in multi-scale layers for further classification.

Second, each object was assigned a pre-defined thematic class label at a hierarchical level based on the membership rule. The colour, shape and contextual information of the objects as well as the ecological and geomorphological characteristics were utilised to develop the rule sets for classification of the geomorphic zone, substrate and habitat classes.

Third, for the classified image, we used visual interpretation; manual and contextual editing method to modify the misclassified objects that mainly due to the thin cloud cover, cloud shadow, stripes on the image and some deep reef features. The Google Earth Imagery and the Landsat8 data were also used as references in the manual editing.

Finally, the classified images were mosaicked to produce the final coastal and marine habitats map, which was then imported to the geographic information system (ArcGIS) for further analysis.

Each image used for the classification was also processed to generate the 0.5-meter panchromatic sharpened image using the Gram-Schmidt method with ENVI software (Laben and Brower, 2000). These pan-sharpened multispectral images were used for validation to evaluate the classification results and for some further modifications.

Classification categories

Class 1	Symbol	Class 2	Symbol	Comment
Any class 1		**Cloud**		
		Waves		
		Distinctive Seagrass/Algae/ Cyanobacteria		
		Unidentified matter or object		
		Circular hole - undetermined origin		
		Unidentified		
		Fishing net		
		Mariculture cage		
		Buoy/Beacon		
		Wreck		

		Sand plume		
Offshore structure		Helipad		
		Lighthouse/Beacon		
		Building/Built structure		
		Construction works		
		Jetty/Pier		
		Harbour works		
Man-made structure (connected to Above water geographic feature)		Runway		
		Jetty/Pier		
		Harbour works		
Seawall				
Non-accessibility device				
Man-made harbour/channel				
Above water geographic feature		Road		
		Runway		
		Helipad		
		Building/Built structure		
		Sand (>10m diameter)		
		Tree		
		Wetland		

		Grass		
		Bare soil/Concreted clearing		
		Barren soil/Sand		
		Seawater intrusion		
		Cultivation		
		Beach rock platform		
		Construction works		
		Tennis court		
		Basketball court		
		Wetland		
Reef flat (incl. reef crest)		**Sand dominant**		Shallower than -3m (below MSL)
		Coral/Seagrass/Algae dominant		
		Degraded		
		Dredged		
		Beachrock platform		
		Seagrass/Algae dominant		
		Man-made track		
Reef slope		**Sand slope**		
		Spur and groove		
		Dredged		
		No class 2	Transparent	

Coral Reef Platform		**Sandy shoal**		Submerged feature with no reef flat
		Spur and groove		
Coral head				(rise to wave base and close to MSL) Between 10m and 150m wide
Lagoon		**Knoll/Seagrass/Algae**		below wave base are knolls <2m deep
		Sandy bottom		
		Coral head (rises to near MSL)		
		Reticulate reef system		
		Coral bottom		Little coral heads visible but no reticulate reef pattern
		Dredged		
		No class 2	Transparent	
Deep water	Transparent (not displayed)			

Limitation of the methodology

The developed classification rule sets can be applied for different study areas and different images, but we need to select the hierarchical level from the multi-scale layers through visual assessment and adjust the threshold values for the membership rules via the trial and error process due to the differences on composition of the reefs, the images quality and environmental conditions.

References

1. Baatz, M., Schäpe, M., 2000. Multiresolution segmentation-An optimization approach for high quality multi-scale image segmentation. In: Strobl, J., Blaschke, T., Griesebner, G. (Eds.), Angewandte Geographische Informations-Verarbeitung XII. Wichmann Verlag, Karlsruhe, pp. 12-23.

2. Benz, U.C., Hofmann, P., Willhauck, G., Lingenfelder, I. & Heynen, M. 2004. Multiresolution, object-oriented fuzzy analysis of remote sensing data for GIS-ready information. ISPRS Journal of Photogrammetry and Remote Sensing. 58, 239-258.
Blaschke, T., 2010. Object based image analysis for remote sensing. ISPRS Journal of Photogrammetry and Remote Sensing 65, 2-16.

3. Laben, C.A. and Brower, B.V., 2000. Process for Enhancing the Spatial Resolution of Multispectral Imagery using Pan-Sharpening. U.S. Patent 6,011,875. Jan 4, 2000.
Trimble eCognition, 2015. eCognition Developer 9.1 Reference Book, Trimble Germany GmbH, Munich, Germany, pp. 67-73.

5. Geographic description

This final step in the study involves the integration of the results of the three scientific investigations (sea level, bathymetry and habitat classification) that provided the basis for the geographic description in the description sheets, which is divided into 4 parts:

1. Geographic area
2. Land area above water
3. Human infrastructure
4. Intertidal and submerged area

The first part provides indications on the physical characteristics of the shallow feature described (oceanic coral reef platform or atoll with a lagoon, for example), its size and its geographic location relative to the surrounding mainlands. Where time series of satellite images accessible online demonstrate that land filling activities have taken place, they are mentioned. The second part provides a geographic description of areas that are above water on the day and time of capture of the satellite data used for the study. This includes a description of the shape and size of these areas as well as their ground cover characteristics (vegetation, sand, beach rock, etc.). It also includes a discussion of the likelihood for small sandy areas that are above water at the time of capture of the satellite data to remain above water at high tide through a comparison with other satellite images of the same feature captured at different moments. The third part is focused primarily on the description of visible human infrastructure (refer to the legend for the Habitat Classification and Land Cover Map for further details on what could be identified). The fourth part describes the intertidal and submerged areas, including the bathymetry profile, shape and size of the different parts of the reef platforms, as well as marine habitat types and the presence of distinctive features (if any). Traces of human activities are also described, including marks left by dredging activities.

For further information on the purpose of each part and assessment methodology, please refer to the User Guide.

This investigation relied on the results of the study, the references listed in the first section of this methodology, and the reference below.

References

1. <<南海诸岛地名资料汇编>>. 广东省地名委员会编, 出版: 广州 : 广东省地图出版社, 1987. Guangdong Province Committee on Geographical Names, 1987. A Collection of Nanhai Islands Geographic Names and Documents, Guangdong Province Map Press, Guangdong (China). pp 629.

2.《南沙群岛空间融会信息剖析与示警：群礁发育、军事区位、警示体系》作者：高俊国，刘宝银 著 出版社：海洋出版社 2009
Gao, Junguo and Liu, Baoyin, 2009. Spratly Islands space fusion and warning information analysis: Group reef development, military location, warning system. China Ocean Press. pp 172.

3. S. Andréfouët et al. (2001) Typology of atoll rims in Tuamotu Archipelago (French Polynesia) at landscape scale using SPOT HRV images, International Journal of Remote Sensing 22(6):987-1004

4. S. Andréfouët et al. (2003) Multi-Site Evaluation of IKONOS Data Classification of Tropical Coral Reefs Environments, Remote Sensing of Environment 88: 128-143

5. P. Blanchon, Geomorphic Zonation of Coral Reefs, in Encyclopedia of Modern Coral Reefs (469-488), available at http://www.academia.edu/421204/Geomorphic_Zonation_of_Coral_Reefs_Encyclopedia_of_Modern_Coral_Reefs

6. Hancox, D. and Prescott, J. R. V., 1995. A geographical description of the Spratly Islands and an account of hydrographic surveys amongst those islands. Maritime Briefing, 1(6) International Boundaries Research Unit.

7. S. Kakuta et al. (2010) Satellite-based Mapping of Coral Reefs in East Asia, Micronesia and Melanesia Regions, International Archives of the Photogrammetry, Remote Sensing and Spatial Information Science, Volume XXXVIII, Part 8, Kyoto Japan 2010 available at http://www.isprs.org/proceedings/XXXVIII/part8/pdf/W06D04_20100311190523.pdf and the corresponding coral reef layers in ArcGIS.

9. W.G.H. Maxwell, Atlas of the Great Barrier Reef, Elsevier Publishing Company 1968.

10. P. Mumby and A. Harborne (1999) Development of a Systematic Classification Scheme of Marine Habitats to Facilitate Regional Management and Mapping of Carribean Coral Reefs, Biological Conservation 88: 155-163

11. P. Mumby and A. Edwards (2002) Mapping Marine Environments with IKONOS imagery: enhanced spatial resolution can deliver greater thematic accuracy, Remote Sensing of Environment 82: 248-257

12. P. Mumby et al. (2004) Remote zsensing of Coral Reefs and their Physical Environment, Marine Pollution 48: 219-228

13. Sailing Directions (Enroute) South China Sea and the Gulf of Thailand, Publication 161, U.S. Governement Printing Office (2013)

14. Satellite imagery of land reclamation by country available online at https://amti.csis.org/island-tracker/ - Also https://medium.com/satellite-image-analysis

15. UK Admiralty Sailing Directions, China Sea Pilot (2010)

16. M.J. Valencia, J.M. Van Dyke, N.A. Ludwig, Sharing the Resources of the South China Sea, University of Hawaii Press, 1997

17. 2014 SRTM15 topography grid made available by the Scripps Institution of Oceanography, University of California San Diego: http://topex.ucsd.edu/WWW_html/srtm30_plus.html

6. Design of web platforms to display the results

Two web platforms have been designed to display the results of the study; one on the website of the Centre for International Law (CIL) here, and the other one on the website of the Centre for Remote Imaging Sensing and Processing (CRISP) here.

CIL's web platform provides access to the 139 description sheets in pdf format for easy reference and printing. They can be accessed through a geographic (or map-based) search, or by alphabetical order.

CRISP web platform displays:

- the habitat classification shapefiles and underlying GIS database,
- geo-referenced bathymetry maps, and
- the geographic descriptions contained in the description sheets.